Fabrication of high aspect ratio Si nanogratings with smooth sidewalls for a deep UV-blocking particle filter

Pran Mukherjee,[a)] Myung-Gyu Kang, Thomas H. Zurbuchen, and L. Jay Guo
The University of Michigan, Ann Arbor, Michigan 48109

Fred A. Herrero
NASA Goddard Space Flight Center, Greenbelt, Maryland 20771

(Received 10 June 2007; accepted 8 October 2007; published 11 December 2007)

To measure space plasmas and neutral particles one must filter out high-energy ultraviolet photons that would increase background count or damage sensors. To enable sensitive neutral particle measurements, a photon-to-particle rejection rate of 10^{14} is desired, far exceeding the requirements of prior filters. The authors propose a high-aspect ratio Si grating with densely packed, sub-100 nm slits. In this article, the authors report the development of a new technique for fabricating sturdy, self-supported transmission gratings in silicon using nanoimprint lithography and deep reactive ion etching, resulting in grating slits with scalloping under 7 nm and high (8.5:1) aspect ratios. © *2007 American Vacuum Society.* [DOI: 10.1116/1.2804612]

I. INTRODUCTION

Composition measurements of plasmas and neutral particle populations in space are part of many satellite missions designed for space weather monitoring and forecasting and exploration of planetary environments and the interstellar medium. The Sun is constantly expelling a high-speed omnidirectional stream of particles called the solar wind. The solar wind is heated and accelerated away from the Sun in a region called the corona, the outer atmosphere of the Sun. The mechanisms dominating this process are so far not understood. *In situ* solar wind measurements are essential for understanding of the heliospheric source region. Such breakthrough measurements will be achieved by the Solar Probe mission,[1] currently under consideration by NASA, which will have a perihelion of only ten solar radii.

Instruments measuring low-density plasmas like the solar wind plasma need to be sensitive to individual particle impacts. However, the vast majority of these instruments rely on sensors that are highly vulnerable to energetic ultraviolet photons, which can degrade the instrument performance or produce noise in the system. In particular, the Lyman-α band of UV (121.6 nm), caused by excited hydrogen emission in the Sun, has an intensity over a thousand times brighter than the surrounding spectral bands. The 10.25 eV Ly-α photons have enough energy to produce a signal that is indistinguishable from the particle signal.[2,3] An ultraviolet rejection rate of at least 10^{14} compared to particles is desirable in order to separate out both ionic and neutral species signals from the background signal, but 10^{10} would suffice for an ion-only sensor. Such high UV rejection has never before been achieved by a grating technique, and suppression factors for prior techniques were rarely measured.

As an alternative to bulky electrostatic light traps, in the late 1990s the Massachusetts Institute of Technology (MIT) exploited dense and deep gold grating structures as UV blocking filters (Fig. 1). Gold gratings with 40 nm slits, 200 nm period, 520 nm depth, and 1.7 cm^2 area were fabricated by a combination of laser-interference lithography for patterning, deep-reactive ion etching (DRIE) to create the high aspect ratio slits in multilayered photoresist, and electroplating to fill the slits with gold.[4] Since gold is very soft, however, an additional nickel support grating was required. These metal grating filters were simulated, built, and flown on the Imaging from the Magnetopause to the Aurora for Global Exploration (IMAGE) mission.[4–8]

These gratings achieved an UV rejection on the order of 10^6 and geometric fill factor of approximately 30%, which was sufficient for the Earth-orbit application. However, since solar UV intensity follows an inverse square radial profile, instruments close to the Sun will require UV rejection factors of $10^{10}-10^{15}$. A gold grating would require slits of at least 800 nm depth and 40 nm width to achieve even the lower end of the required rejection specification (Fig. 2), and the far stronger nickel requires similar geometry in addition to the problem of its intrinsic stress. The electroplating technique used by the MIT group[4] is not able to achieve this geometry because the photoresist lines collapse with depths over 600 nm.

Here we propose a new silicon-based approach to create UV-blocking filters transparent to atoms and ions. Very narrow, high aspect ratio features are needed to block the Ly-α photons, while offering the additional advantage of collimating the solar particles as they pass through the filter. Since silicon has a Young's modulus close to that of stainless steel or nickel, the grating should be able to support itself.

II. EXPERIMENTAL DESIGN

For the new approach we propose, deeply etched bulk silicon forms the grating without the use of a conductive layer. As a semiconductor, silicon has enough free carriers to serve as an ultraviolet filter provided that the features are sufficiently narrow and deep. Simulations (Fig. 2) predict

[a)]Electronic mail: pran@umich.edu

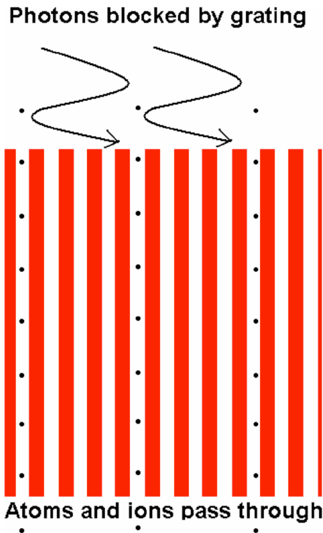

FIG. 1. Grating schematic. Collimated particles flow through narrow, high aspect-ratio grating slits while photons with wavelengths greater than the slit width are absorbed.

that a Si nanograting with a depth of 1.5–2.5 μm and slit widths of 40 nm will provide sufficient attenuation of Ly-α light, exceeding the requirement of current filters. It should be noted that Si gratings, unlike Au, preferentially block the TM mode of light and thus TE mode transmission is the limiting case. There is a significant jump in TE transmission for a slit width variation of just 10 nm, which thus requires significantly greater depth to achieve the same level of rejection of the deep UV photons. Incoming particles must be collimated into beams under 3° wide to penetrate the grating perpendicular to the slit direction. A device of at least 4 cm^2 is desired with as high geometric open area and UV rejection as possible.

Since the purposes of space-based particle sensors include both mass spectrometry and energy detection, it is desirable that particles not be scattered significantly in the process of measurement. Thus it is necessary that any detected particles pass through the grating slits, not the grating lines. A simulation using the Stopping Range of Ions in Matter (SRIM)[9] program modeled the penetration of a variety of ions through a 1.5 μm thick sheet of silicon. Since a grating is not a solid sheet, the simulated penetration depths were doubled for safety, and even so no ions with energy under 20 keV/nucleon penetrated the grating. Since the solar wind is typically 1–2 keV/nucleon, only shock-accelerated particles and the rare high-energy cosmic rays will penetrate the grating's solid pieces, making silicon an acceptable material for the application.

The most challenging task in creating such a structure is to achieve dense and deeply etched Si trenches with very smooth sidewalls. While the desired high aspect ratio ($\sim$40–50) is achievable with DRIE tools by using alternating etch and passivation steps,[10] the scalloping (well over 100 nm) normally associated with such techniques needs to be minimized or eliminated in order to obtain dense and deep slits with sub-100 nm width. The effect of even 10 nm slit width

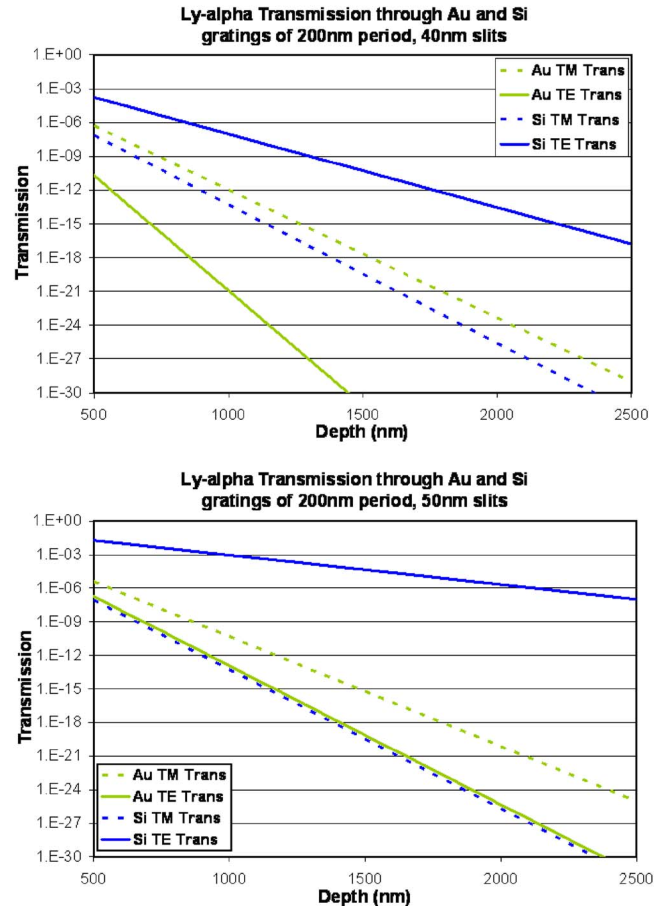

FIG. 2. Simulated transmission characteristics of the transverse electric and transverse magnetic modes of 121.6 nm Lyman-α light through Si and Au nanoscale gratings with 200 nm period and slits of 40 and 50 nm width. The dark lines correspond to Si gratings and the light to Au, solid lines for TE transmission, and dotted lines for TM.

variation mentioned earlier, along with the necessity of allowing incoming particles to penetrate the grating unimpeded, limits scalloping to no more than 20% of the slit width. Hence, a 40 nm slit should have no more than 8 nm scalloping on each sidewall.

We utilized nanoimprint lithography (NIL) to provide the grating pattern and high aspect ratio silicon DRIE to etch the gratings (Fig. 3). DRIE will also be used for the back etch to create freestanding structures. NIL has the advantages of high resolution and high throughput, while a modified Bosch process DRIE using high oxygen content provides a smooth etch.[11] Use of a silicon-on-insulator wafer would provide etch stops for both grating and backside etches. In the work presented in this article, 200 nm period Si nanograting with sidewall scalloping roughness below 7 nm was achieved using an inductively coupled plasma (ICP) etcher with SF_6+O_2 etch chemistry and C_4F_8 passivation. The primary quality factors for such an etch technique are patterning speed, pattern repeatability, fill factor, and the self-supporting nature of the grating.

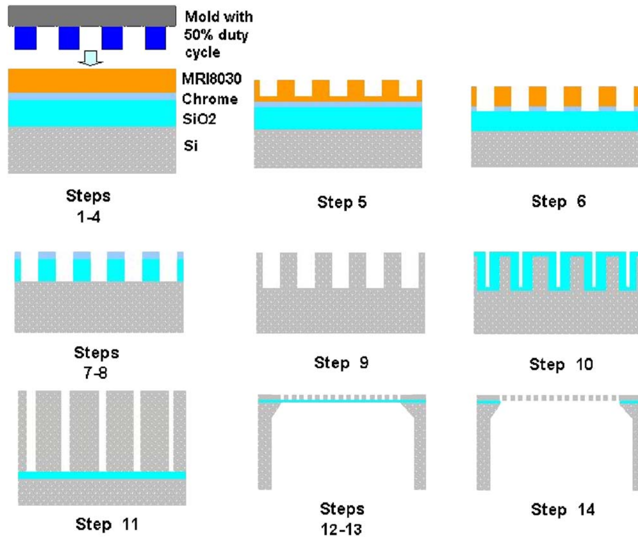

FIG. 3. Process flow for grating fabrication. Steps are: (1) Make or buy silicon-on-insulator wafer, (2) grow 200 nm mask oxide, (3) evaporate 10 nm chromium, (4) deposit thermal polymer (MRI 8030), (5) nanoimprint grating into polymer, (6) polymer residual etch and chromium etch, (7) remove polymer, (8) dry-etch mask oxide, (9) STS etch grating, stage 1, (10) dry oxidize sample to narrow grating lines and create second-stage etch mask, (11) STS etch to buried oxide etch-stop, (12) STS etch backside 80% through wafer, (13) chemical etch through to etch stop, and (14) dry-etch oxide.

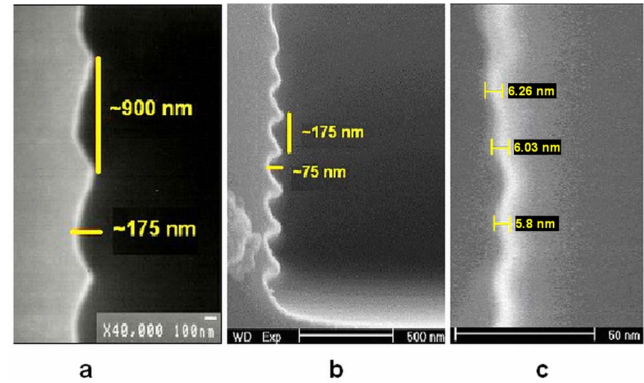

FIG. 4. Scalloping of DRIE etches. (a) The standard Bosch process results in large, deep scallops. (b) Our initial tests with SF_6+O_2 etch chemistry reduced scalloping significantly. (c) Our current process results in less than 7 nm scalloping over a vertical etch of 15 nm.

III. RESULTS AND DISCUSSION

Initial DRIE characterization on an STS MESC Multiplex ICP using 2 μm half-pitch features demonstrated that increased oxygen content both reduced scalloping significantly and reduced the silicon etch rate (Fig. 4). While etch rates for a standard Bosch process on this tool can be $2-5$ μm/min, adding 60% O_2 reduced that to 0.41 μm/min, and 80% O_2 resulted in 0.17 μm/min. However, the latter case also resulted in sidewalls with under 7 nm scalloping, and since our target features are on the order of 2 μm deep that etch rate is sufficient.

Further experimentation with etch parameters resulted in the following observations:

(1) The ratio of etch time versus passivation time affects feature profiles, but not scalloping. Overpassivation results in features narrowing toward the bottom since the etch fails to completely remove the passivation layer, and underpassivation results in widening features as the plasma etches past the passivation a little more each cycle.

(2) Absolute gas pressures during etching affect feature profiles significantly, but not scalloping. The same reason applies as earlier, since during the etch step the amount of oxygen in the mixture determines the self-passivation rate (i.e., sidewall oxidation). The oxidation has a higher efficiency than the SF_6 etch, so for example doubling both gas flow rates will result in overpassivation and features will narrow as they go deeper.

(3) Gas ratio during etch affects scalloping, but not feature profiles. This is because the gas ratio determines the rate that the self-passivation is removed. An ideal gas mixture will self-passivate the sidewalls exactly as fast as it etches them to maintain smoothness but not overpassivate. The primary etching should be downward, not sideways. It should be noted that the gas ratio seems to primarily affect the bottom of the features (i.e., the portion immediately being etched) whereas absolute gas pressure and etch/passivation time ratio seem to affect the entire feature.

(4) Absolute etch time per cycle affects scalloping; lower etch times per cycle result in smaller scallops.

(5) The SF_6 valve must remain slightly open at all times, even during passivation, since otherwise the low flow during the etch stage results in the valve occasionally sticking between passivation and etch steps, causing non-deterministic etch profiles.

These observations were valuable for maximization of etch rate and selectivity while maintaining straight sidewalls. In addition, they enabled us to set a starting point for future parameter ramping during extremely high aspect ratio etching.

The 2 μm half-pitch etch characterization showed that smooth, straight sidewalls were possible. Experiments with nanoimprinted gratings of 350 nm half-pitch resulted in significantly higher aspect ratios, and our first 100 nm half-pitch gratings (Fig. 5) still had vertical sidewalls with excellent smoothness and straightness. However, in the latter case the masking oxide layer charged up during the etch and led to significant mask undercutting ($\sim$35 nm). This will be mitigated in the future by a less aggressive etch at the beginning of the process, using an even lower SF_6 component and higher platen bias for enhanced directionality.

Where the relatively large feature sizes defined by optical lithography allows one to use thick oxide masks etched with buffered hydrofluoric acid, the smaller features of nanoimprint lithography require the control of a dry etch. Since dry oxide etches have low selectivity to photoresist, and imprint molds are on the order of 200 nm deep, this limits us to oxide layers of 200–300 nm thickness.

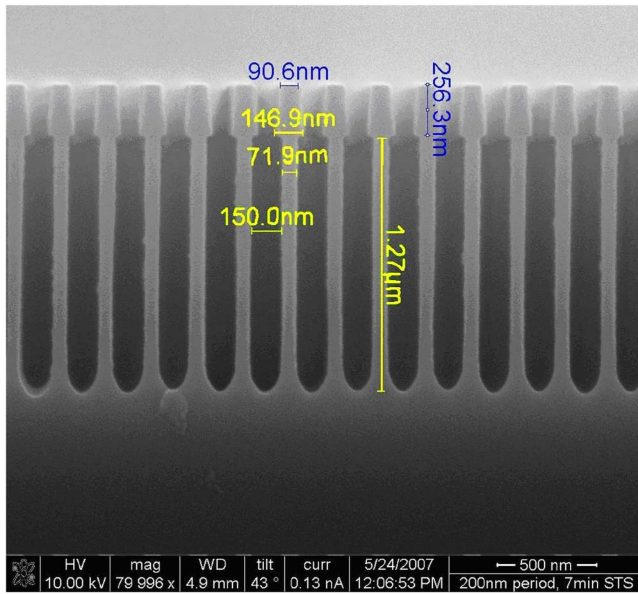

FIG. 5. This grating was created from a 115 nm half-pitch mold following the process in Fig. 3 through stage 9. After the oxide hard-mask was created, a 7 min STS DRIE etch (described in Section III) resulted in 1.27 μm deep grating lines (etch rate: 0.18 μm/min). The early 35 nm mask undercut widened the initial lines to 150 nm, leaving an aspect ratio of 8.5:1.

For a typical Bosch etch, even a thin oxide layer provides a sufficient mask since the fast silicon etch rate results in oxide-to-silicon selectivity on the order of 100:1. The oxygen in our modified etch chemistry slows down the silicon etch rate by a factor of 20 or more without slowing down the oxide etch rate. In fact, we increased the oxide etch rate by using high platen power during both etch and passivation steps (25 and 30 W, respectively), which is not normally done. Experiments proved that reducing the platen power to 15 W during etch and 0 W for passivation increased our selectivity by 88% by bringing oxide etch rates back in line with Bosch process standards. Our initial supposition that the oxide was additionally etched by loss of the C_4F_8 passivation layer during switching proved unfounded, since decreasing the cycle time had minimal effects on oxide loss rates.

IV. CONCLUSIONS

We explored high aspect-ratio etches to create UV-blocking transmission gratings with high geometric open area. The deep ion etch technique we developed is self-passivating during the etch stage, and thus results in sidewall roughness under 7 nm. Our first tests resulted in 8.5:1 aspect ratio slits, and our technique shows promise for gratings with slit width under 50 nm and aspect ratios of up to 40:1. This would be valuable not just for this application, but also others such as birefringent wave plates, high aspect ratio NIL molds, collimators, polarizers, x-ray diffraction plates, and more.

ACKNOWLEDGMENTS

This work is supported by NASA under Grant No. NNG04GL44H. The authors would also like to thank Jin-Sung Kim for providing the 200 nm period molds and the staff of the Michigan Nanofabrication Laboratory for their assistance with tools and process parameters.

[1]See http://solarprobe.gsfc.nasa.gov/.
[2]T. Zurbuchen, P. Bochsler, and F. Scholze, Opt. Eng. **34**, 1303 (1995).
[3]W. Curdt, P. Brekke, U. Feldman, K. Wilhelm, B. N. Dwivedi, U. Schühle, and P. Lemaire, Astron. Astrophys. **375**, 591 (2001).
[4]J. T. M. van Beek, R. C. Fleming, P. S. Hindle, J. D. Prentiss, M. L. Schattenburg, and S. Ritzau, J. Vac. Sci. Technol. B **16**, 3911 (1998).
[5]M. M. Balkey, E. E. Scime, M. L. Schattenburg, and J. van Beek, Appl. Opt. **37**, 5087 (1998).
[6]C. J. Pollock *et al.*, Space Sci. Rev. **91**, 113 (2000).
[7]M. A. Gruntman, Appl. Opt. **34**, 5732 (1995).
[8]E. E. Scime, E. H. Anderson, D. J. McComas, and M. L. Schattenburg, Appl. Opt. **34**, 648 (1995).
[9]SRIM, see www.srim.org.
[10]A. A. Ayón, R. Braff, C. C. Lin, H. H. Sawin, and M. A. Schmidt, J. Electrochem. Soc. **146**, 339 (1999).
[11]H. Kawata *et al.*, Jpn. J. Appl. Phys. **45**, 5597 (2006).